Multiple interactions between molecular and supramolecular ordering

M. Manno,[1,2,3] A. Emanuele,[1,2] V. Martorana,[1,3] D. Bulone,[1,3] P. L. San Biagio,[1,2,3] M. B. Palma-Vittorelli,[1,2] and M. U. Palma[1,2,3]

[1]*Progetto Sud (INFM, European Union) I-90123 Palermo, Italy*

[2]*Department of Physical and Astronomical Sciences, University of Palermo, Via Archirafi 36, I-90123 Palermo, Italy*

[3]*CNR Institute for Interdisciplinary Applications of Physics, Via U. La Malfa 153, I-90146 Palermo, Italy*

(Received 13 July 1998; revised manuscript received 16 September 1998)

We report studies of the interplay among processes of molecular conformational changes, spinodal demixing of the solution, and molecular crosslinking involved in the physical gelation of a biopolysaccharide-water system. Multiple interactions and kinetic competition among these processes were studied under largely different absolute and relative values of their individual rates by appropriate choices of the quenching temperature at constant polymer concentration. Quenching temperature strongly affects the rate of growth but not the final value of the fractal dimension of the gel. Kinetic competition plays a central role in determining the final conformation of individual molecules and the structure and properties of the final gel. This behavior highlights the frustrated nature of the system, and the need of bringing kinetics sharply into focus in gelation theories. General aspects of the present findings and, specifically, the interplay of molecular conformation changes, solution demixing, and molecular crosslinking extend the relevance of these studies to the fast growing field of amyloid condensation and Prion diseases. [S1063-651X(99)10202-2]

PACS number(s): 87.10.+e, 82.70.Gg, 87.15.Nn, 61.43.Hv

I. INTRODUCTION

Among ordered supramolecular structures, the case of gels is unique for being topologically characterized by molecular crosslink connectivity. Self-assembly of biomolecular hydrogels is highly relevant to many fields, spanning from polymer science and technology to statistical mechanics and biology [1–3]. Self-assembly often involves an interplay among biomolecular conformation changes, solution demixing, and molecular crosslinking, as also observed in some polypeptide/protein cases [4–8]. The fact that conformational changes are also required in the case of protein coagulation and related amyloid deposition [9] extends the relevance of the present studies to the fast growing field of amyloidoses and Prion diseases.

The sol gel transition was originally modelled in terms of the Flory-Stockmayer-Gordon infinite cluster [10]. Later, it was successfully modelled within the topological universality class of percolation [2,11]. Early observations of concentration inhomogeneities in the gel state already suggested that gelation processes should somehow be considered jointly with solubility [12] and demixing [13]. Nevertheless, early studies, as well as further experimental and theoretical ones, were focused on final equilibrium states, kinetic considerations being only inferred and observations extended at most to part of the process [12–15]. Evidence for a spinodal process in an early stage of gelation (undistinguished, however, from gelation itself) was provided by Feke and Prins [14]. Complete kinetic studies of phase separation were initially performed on simple cases such as entanglement of rodlike polymers [16] or transient percolation of simulated clusters [17], that is on self-assembly due to one single process. Extended kinetic studies on systems undergoing both gelation and phase separation, carried out since 1985, have allowed a clear identification of the *dramatis personae* of hydrogel self-assembly, that is of the distinct processes concurring in it [18].

The first process (important at not very high concentrations) consists in the formation of a biphasic mesoscopic pattern of high and low concentration domains in the solution, due to a liquid-liquid phase separation. This separation occurs when the solution is brought either in its thermodynamically unstable region (spinodal demixing) or in its metastable region (nucleated demixing) [5–8,18–20]. The mechanism includes the case of critically divergent fluctuations of sufficient amplitude and life time (transient demixing), occurring on approaching the instability region of the sol as such [4].

The second process is that of multiple molecular crosslinking, which is possible when individual solute molecules exhibit multiple sites for linking [21], and it is preferentially triggered in high concentration domains. Such crosslinking can be nucleated and sometimes it can be autocatalytic [22], but in no way its nucleation should be confused with that of nucleated demixing.

The third process, often also involved, is that of molecular conformational change [23–26]. This process shares with that of mesoscopic demixing a thermodynamic drive towards configurations (in this case, molecular conformations) offering more advantageous interactions within the (solute+solvent) system. Consequently, demixing and conformational changes can be expected to interact. This and the already recalled effect of demixing on crosslinking shows that the three mechanisms can be multiply interconnected.

These processes were identified in previous work [4–8,18–20]. Their simultaneous interactions and kinetic competitions are here studied for the first time. To this purpose we have chosen aqueous solutions of Agarose, an uncharged biostructural polysaccharide [23] often used in studies of physical gelation [6–8,14,18–20,23,24,26–29]. The phase diagram of the system is reported in Fig. 1, where

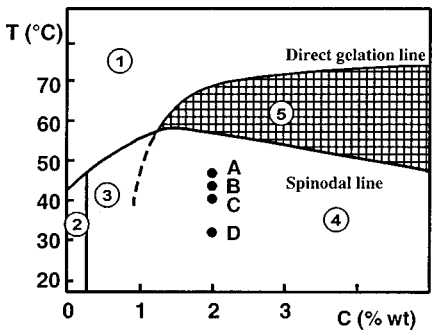

FIG. 1. Phase diagram of agarose-water systems (redrawn from Ref. [8]). (1) Thermodynamically stable sol. (2) Mesoscopic gel. Freely drifting mesoscopic regions of gel are formed, while the sample remains macroscopically liquid. (3) Spinodal promoted gel. (4) Gel formed as a result of kinetic competition among demixing, conformational transition and crosslinking. $A-D$ indicate quenching points used in the present work. (5) Direct gelation region.

regions 2–5 refer to different gelation pathways. For this reason, the diagram reflects not only equilibrium but also (to some extent) different kinetic conditions and corresponding different texture and features of the final gels. As is already known, at very low concentrations (region 2) spinodal demixing of the sol occurs first and it generates mesoscopic domains of a high concentration minority phase. In those conditions, gelation and implied molecular conformational changes follow at a later time within the high concentration mesoscopic domains [8,20]. Since the latter are unconnected at these low average concentrations, their internal (mesoscopic) gelation does not destroy the fluidity of the sample [20]. At intermediate concentrations (region 3), again spinodal demixing promotes and is followed at a later time by molecular crosslinking and related conformational changes [6(b),(c)]. At variance with region 2, however, gelating domains now form a percolating pattern which allows true macroscopic gelation [6,8]. Such clear-cut time resolution of demixing, molecular conformational changes, and crosslinking processes is not necessarily observed in region 4, where strong mutual interactions and kinetic competition (depending on specific conditions) are expected [19].

For this reason in the present work we have studied gelation kinetics for quenchings to appropriate points in region 4 of the phase diagram (points $A-D$ in Fig. 1). Changing the quenching temperature *ceteris paribus* allowed studying kinetic competition among the three processes under widely different absolute and relative values of their individual rates. Results show how this modulation of interactions and kinetic competition generates large diversities in molecular conformation and larger-scale structural properties of gels. These diversities highlight the frustrated nature and the complexity of the system as well as the complexity of interactions among processes. However, out of those complexities simple features such as correlation length, order (or, better, nonrandomness) parameter, and fractal dimension of the structure of crosslinked polymers emerge, with their own kinetics. The fractal dimension of this structure is seen to play in gelation a role as important as that of topology. A partial report on this particular aspect has been recently published [27]. The present results emphasise the need for taking centrally into account kinetic processes in gelation theories.

II. MATERIALS AND METHODS

The material used in our experiments was Agarose, an uncharged polydisaccharide. We used Seakem HGT(P) Agarose, from BioProduct, Marine Colloids Division, having sulphate content less than 0.15%, molecular weight 120.000 and polydispersity not larger than 10%, as estimated from previous dynamic light scattering experiments [6(a)]. Powder was dissolved in Millipore (SuperQ) water for 20 min at 100 °C, filtered at 80–90 °C through 0.22-μm filters and poured directly in the thermostatted (cylindrical) measuring cell. As previously reported, the whole phase diagram of the system is to some extent sensitive to the particular HGT(P) bath of Agarose. However, this amounts to very minor displacements of, e.g., the spinodal line, within a temperature range of approximately 1 °C, while the general behavior of this HGT material remains essentially unchanged.

Optical rotation dispersion (ORD) measurements were performed at $\lambda = 589$ nm, with a Jasco DIP 370 digital polarimeter using a temperature controlled quartz cell of 5 cm path length.

For viscoelastic measurements a Rheometrics viscoelastic spectrometer was used, with a couette-type setup, a rotating cylindrical cup and a measuring inner coaxial air-suspended bob with a 1-mm gap. Viscoelastic spectra over four orders of magnitude were obtained using a multiple frequency strain. Using this operating mode, the specimen is subjected to a small strain containing up to eight octaves. Two such strains covered therefore (with some useful overlap) the four frequency decades shown in our figures. In this way, data relative to any given kinetic ''point'' were obtained over the four decades in about 100 sec. The strain amplitude was below 1% so that perturbation was negligible and the entire set of measurements relative to one kinetic could be performed on one and the same specimen. For quick determination of the gel point, we also used the classical drop-ball method by gently releasing a steel ball (about 70 mg weight) on the surface of gelling specimens, at different times.

For light scattering experiments we used a Spectra Physics 2020 argon laser tuned at 514.5 nm or a Spectra Physics model 127 helium-neon 628.3-nm laser. Data were automatically collected at different angles using a Brookhaven BI-200SM goniometer and a 128-channel Brookhaven BI-30AT correlator. When dealing with gels or, in general, with nonergodic samples [30], a motor-driven cell holder was used to scan different regions of the specimen, thus allowing ensemble averaging.

For small angle light scattering (SALS) measurements we used a charge coupled device (CCD) Panasonic camera [31]. A lens between the sample cell and the detector provided a one-to-one correspondence between a circular ring on the CCD screen and the scattering vector $q = 4\pi n \lambda_0^{-1} \sin(\vartheta/2)$, where n is the medium refractive index of the sample, λ_0 is the wavelength of the incident laser light and ϑ is the scattering angle. Spatial integration through the sample was obtained by expanding the incident laser beam. Actually, the CCD was shifted off-axis so as to avoid direct exposure to high laser intensity while doubling the available angular span. The structure function (scattered intensity versus scattered vector q) was obtained by integration along circular sectors.

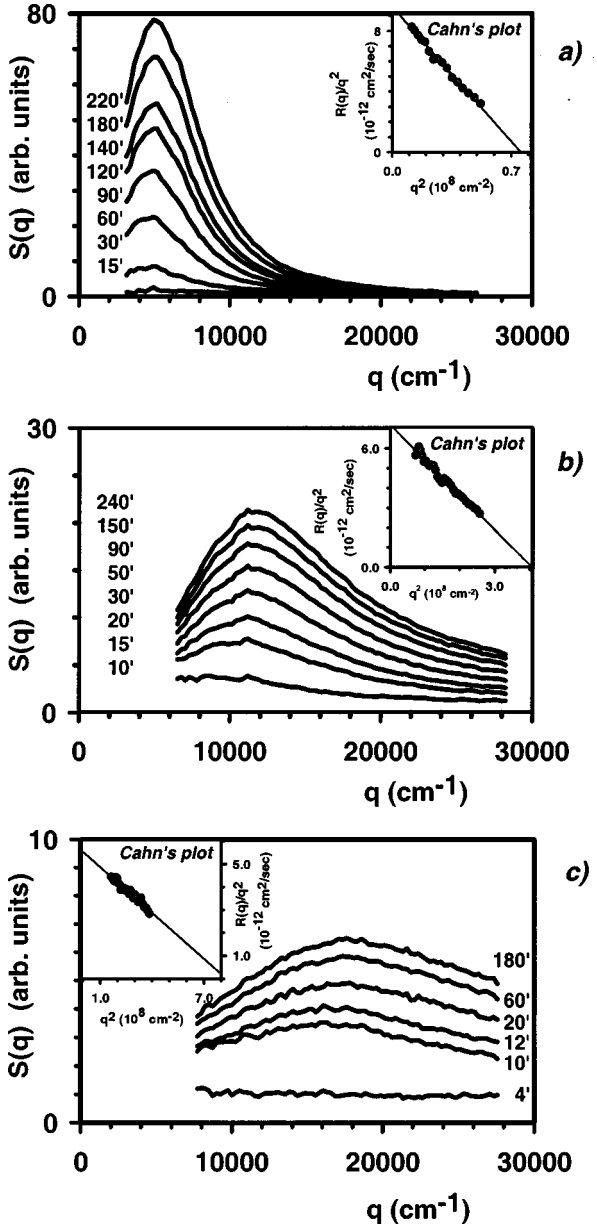

FIG. 2. Structure functions $S(q)$ at different times after quenching to (a) point *A*; (b) point *B*; (c) point *C*, where *A*, *B*, and *C* are shown in Fig. 1. Cahn's plots are given in the insets. Growth factors $R(q)$ are obtained from exponential growths of the scattered intensity.

Combination of large and small angle scattering setups allowed to follow the time evolution of the structure function $S(q)$ in the q range 3000–300 000 cm^{-1}.

III. EXPERIMENTAL RESULTS

Samples of 2% wt. Agarose in water were quenched from 80 °C to points $A-D$ in region 4 of the phase diagram in Fig. 1, and the time evolution of the following quantities was recorded: (i) $S(q)$, monitoring demixing on a scale length of $20 \div 2\ \mu$m (low angle scattering); (ii) optical rotation, monitoring conformational changes; (iii) viscoelastic response, monitoring conformational changes, crosslinking, and gelation; (iv) fractal dimension of the system on a scale length of $1 \div 0.1\ \mu$m (large angle scattering), that is in the range of lengths well below that of the narrow distribution of sizes of demixed droplets.

TABLE I. Structural parameters relative to quenchings to points *A*, *B*, and *C* in Fig. 1; T_Q, quenching temperature; q_m, scattering vector corresponding to the maximum of the structure function; $L_m = 2\pi/q_m$, correlation length; d_g, final value of the fractal dimension. $S(q_m)_{\text{fin}}$, value of the peak of the structure function at the end of the experiment. Δ ORD, total change in the optical rotation dispersion signal.

	T_Q (°C)	q_m (cm^{-1})	$L_m = 2\pi/q_m$ (μm)	d_g	$S(q_m)^{a}_{\text{fin}}$	$[\Delta\alpha]^{b}$
A	46.5	5000	12.5	1.4	80	0.1
B	43	12 000	5.2	1.4	20	0.25
C	40	17 000	3.7	1.2	6	0.75
D	31.5	No maximum observed		1.2		1.1

[a]These values, reported for comparative purposes only, were measured at the end of each experiment. Not necessarily they express saturation values (compare with Fig. 10).

[b]$[\Delta\alpha] = \Delta\alpha/cd$, where $\Delta\alpha$ is the observed rotation angle in degrees (initial value subtracted), c is the solute concentration (2×10^{-2}), and d is the optical path (5 cm).

A. Kinetics of demixing

Upon quenching to points $A-C$ all typical features of the early stages of spinodal demixing are observed, as described by the Cahn-Hilliard linear regime equations [32]:

$$\frac{dS(q)}{dt} = 2R(q)S(q) \quad \text{and} \quad \frac{R(q)}{q^2} \sim 2q_m^2 - q^2. \qquad (1)$$

From Fig. 2 we see that structure functions show maxima revealing the existence of patterns of domains of higher- and lower-than-average concentration, characterized by a correlation length $L_m = 2\pi/q_m$. Here q_m indicates the q value corresponding to the maximum of S_q and L_m is of the order of several micrometers (Table I). The linear regime, monitored by the exponential growth of scattered light (data not shown) and by Cahn plots (Fig. 2, insets), proceeded up to a time t_c (Table II). Coarsening and related dynamic scaling regime predicted for later stages of spinodal demixing in simple systems [33] was not observed, as Fig. 2 clearly shows. This agrees with the already established fact that the length scale of the demixed pattern is frozen in by gelation at

TABLE II. Characteristic times of kinetics relative to quenching to points $A-D$ in Fig. 1; T_Q, quenching temperature; t_C, duration of Cahn's linear regime; t_g, time of macroscopic gelation; Δt_{OR}, time interval of optical rotation growth.

	T_Q (°C)	t_c (min)	Δt_{OR} (min)	t_g (min)
A	46.5	50	22–240	60
B	43	12	2–30	22
C	40	7	0–20	17
D	31.5	Not measurable	0–9	9

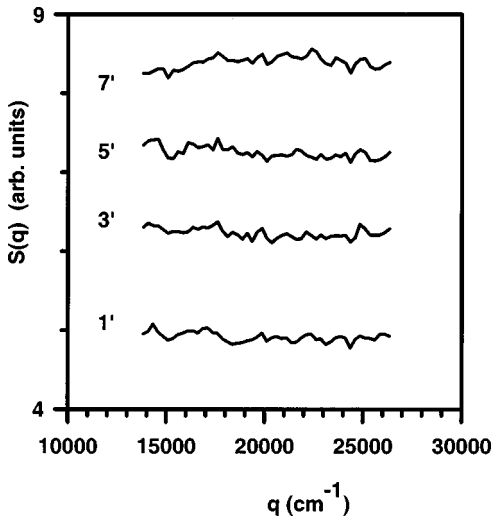

FIG. 3. Structure functions $S(q)$ at different times after quenching to point D of Fig. 1. No indication of spinodal demixing appears in this case.

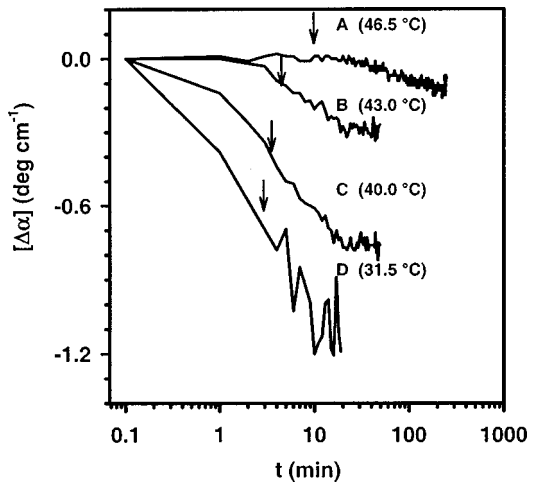

FIG. 4. Change of the ORD vs time after quenching to points $A-D$ of Fig. 1. Arrows mark the onset of gelation revealed by the ball-drop method. ORD tracings are interrupted when measurements become less reliable as a consequence of the sensitivity of the instrument to even slight turbidity. In the figure it is $[\Delta\alpha] = \Delta\alpha/cd$ (initial value subtracted), where c is the weight to weight polymer concentration (2×10^{-2}) and d is the optical path (5 cm). Note that the final value of $[\Delta\alpha]$, observed after quenching in D coincides with the value reported in Ref. [23].

the end of the linear regime and it suggests that this freezing-in makes the linear regime shorter [5,8,18,19,27,33,34]. The intensity of the whole pattern of scattered light, however, increased further with a saturating behaviour, after freezing in. Data on $S(q_m)$ at the end of each experiment are given in Table I. They are useful for comparison purposes, but do not represent absolute or saturation values. For decreasing quenching temperatures, the correlation length and the final value of $S(q_m)$ (Table I) and the time duration of the linear regime t_c (Table II) were seen to decrease. As shown in Fig. 3 and in accord with the general trend in Fig. 2, neither a peak in $S(q)$, nor exponential growth of the scattering intensity are observed upon quenching to point D.

B. Kinetics of conformational changes

No general consensus seems to exist concerning the type of helical polymer conformation in the gel [23–25,29]. However, independently of the specific model, gelation implies a change towards a higher helical content. The early evidence for double helix formation [23,24] and related role of kink sites in the self assembly of a crosslinked structure, does not need to oppose more recent results suggesting the existence, or coexistence of single-helix structures [25,29]. In any case, the present results and conclusions drawn from ORD data, are in no way based on a specific (double/single helix) model.

In Fig. 4 we show ORD changes consequent to quenchings to points $A-D$ and corresponding to changes of helical contents. Tracings in Fig. 4 are interrupted at a point where the increased turbidity might compromise the reliability of measurements. The start and time span of such measured changes and their dependence upon quenching temperatures are reported in Table II. As data in Table I and Table II show, significantly larger helical contents, measured by ORD changes, and correspondingly shorter time spans are observed at decreasing quenching temperatures.

C. Kinetics of viscoelastic properties

For quenching to point A, kinetics are sufficiently slow to allow time resolved viscoelastic studies. Before the onset of coil-to-helix transitions (and consequent gelation) the elastic modulus G' shows a plateau in a narrower frequency region. In Fig. 5(a) this region is $0.1<\omega<10$ rad/s. This behavior is characteristic of entangled polymers with a short relaxation time of about 0.1 s and a reptation time lower than 10 s [35,36]. The higher-frequency behavior agrees with the Zimm model, taking into account hydrodynamic interactions and predicting a $\omega^{2/3}$ dependence of both G' and G'' [37]. As gelation and related helix formation progress, the plateau expands so as to cover the entire available range of frequencies [Figs. 5(b), 5(c) and 5(d)]. The short relaxation time becomes progressively shorter until it becomes no longer observable. This is consistent with a progressively higher rigidity due to the increasing helical content and crosslinking, leading to gelation. The overall progressive tendency towards a solidlike behaviour is also evidenced by the accompanying decrease of the G''/G' ratio, shown in Fig. 6. This starts immediately after quenching, so indicating that crosslinking starts equally soon. The time of macroscopic gelation t_g (monitored by the drop-ball method) is shown by an arrow in the figure and reported in Table II. Similarly to other relevant times, t_g is seen to decrease at decreasing quenching temperatures. Results relative to quenchings in B and C show features qualitatively similar to the A case, except for the already mentioned large differences in final G' values.

In Fig. 7 we show that viscoelastic spectra measured at the end of the experiments of Fig. 2, are flat over the entire available range of frequencies ($0.01<\omega<100$ rad/sec). The ratio G''/G' of the viscous modulus G'' to the elastic modulus G' remains in all cases below the minimum detectable value (10^{-2}). This reflects a solidlike behavior at least in

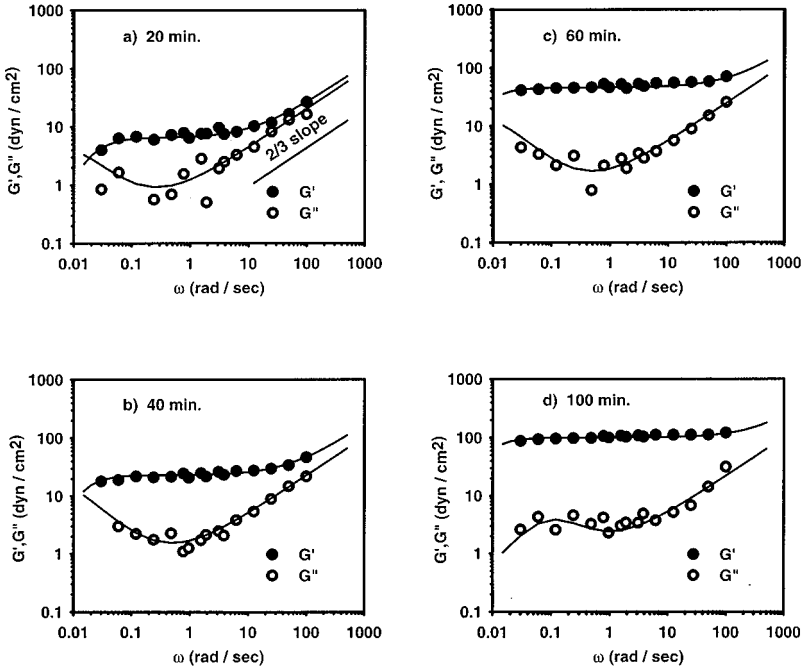

FIG. 5. Viscoelastic spectra at different times after quenching to point *A* of Fig. 1 (46.5 °C). G' and G'' are the real and imaginary part of complex viscoelasticity modulus. Solid lines show the behavior predicted for reptation. Their asymptotic behavior agrees with the Zimm theory [36]. (a) 20, (b) 40, (c) 60, and (d) 100 min after quenching.

this ample range of strain frequencies. Final G' values are seen from the figure to increase over two orders on magnitude from quenching to point *A* to quenching to point *C*. Data relative to point *D* are not equally good, because crosslinking starts immediately and proceeds rapidly at this temperature (see Fig. 4). However, they indicate a further increase of G', approximately over an additional order of magnitude.

D. Kinetics of fractal dimension growth

Formation of demixed droplets takes place on the length-scale $L_m = 2\pi/q_m$ reflected by the peak of the structure function (Fig. 2). For quenchings to points *A*, *B*, and *C*, gelation occurs not much after the end of the Cahn-Hilliard linear regime (Table II) and it freezes the size distribution of demixed droplets. For this reason coarsening is not observed. For point *D*, the faster kinetics prevents even the observation of the linear regime. The size of L_m is of the order of several micrometers (Table I). Polymer conformational changes towards helical forms take place on a smaller scale $L_p \leqslant 0.1\ \mu$m [19] while related crosslinked structures extend up to L_m and beyond. In the interval between L_p and L_m or, more correctly, between L_p and $L_c = L_m/\sqrt{2}$ no special length characterizes the system, either in the gel or in the demixed sol. Accordingly, well within the corresponding q interval $\sqrt{2}L_m^{-1} < q < L_p^{-1}$ the structure function $S(q)$ is seen to be featureless, and log-log plots of $S(q)$ are accurately represented by a straight line, as shown in Fig. 8 [27]. The system is thus self similar in this scale interval. We confine to this interval our observations and plots such as in Fig. 8, because at shorter distances we would probe the individual molecular structure and on a coarser scale we would probe

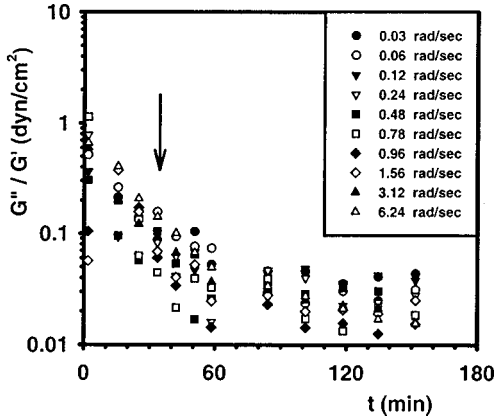

FIG. 6. Ratio between imaginary and real parts of the viscoelastic modulus at different values of frequency, vs time, after quenching to point *A* of Fig. 1. The arrow marks the onset of gelation revealed by the ball-drop method.

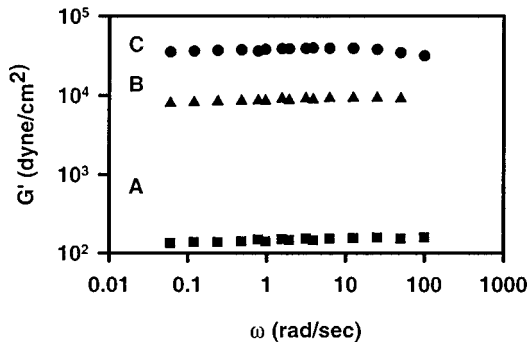

FIG. 7. Elastic modulus, G' vs frequency for samples quenched to *A*, *B*, and *C* at the time of the end of experiments of Fig. 2, that is, well after the gelation time indicated by the ball-drop method. In all cases, G''/G' is less than 10^{-2}. Note the strong dependence of the rigidity of the gel upon quenching conditions.

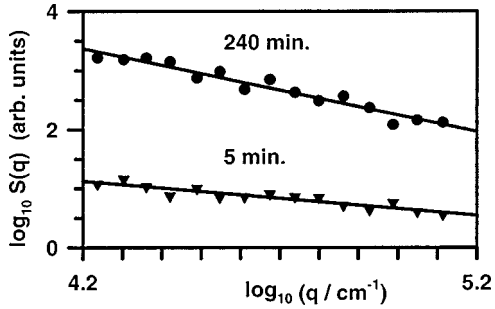

FIG. 8. Log-log plots of structure functions in the 0.1–1 μm interval at different times, after quenching to point *B* of Fig. 1. Straight lines are best fittings.

both the structure of crosslinked polymers and its ''frozen'' spatial modulation due to the initial demixing of the sol. From slopes in Fig. 8, that is, from the power-law dependence:

$$S(q) \approx q^{-d_f} \tag{2}$$

of the structure function upon q, the quantity d_f is derived. This quantity [38] is defined so that the mass M of polymer molecules within a radius $r > L_p$ is $M \approx r^{d_f}$. During the entire course of the experiments and for quenchings to any of the $A-D$ points the power law [Eq. (2)] is observed, with a kinetic progression of the d_f value. The latter is initially very low. This implies a topological dimension $d_T = 0$, corresponding to unconnected scattering objects [27]. At subsequent times, it keeps increasing up to a final value $d_g = 1.3 \pm 0.1$ at the gel point (Table I), irrespective of quenching temperature. This final d_g value is still low, in agreement with the spanning structures observed in agarose gels and related capacity of agarose to make firm gels even at very low concentrations. In Fig. 9, fractal dimension kinetics (preliminarily reported in Ref. [27]) are shown in a unified plot for quenchings to points $A-D$. In the Figure we have rescaled the kinetic observation time against gelation time (t/t_g) and the fractal dimension against its constant value at and after gelation (d_f/d_g). This allows a unified view of fractal dimension kinetics and an operational definition of ''gel point'' in terms of geometric rather than rheological or topological properties.

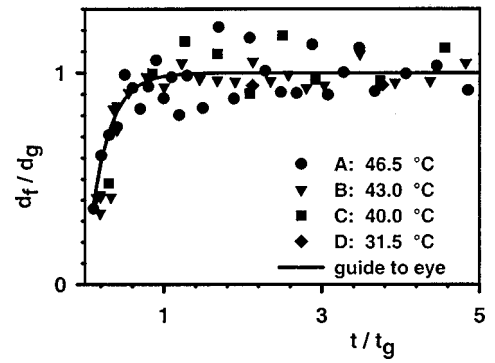

FIG. 9. Rescaled plot of fractal dimension d_f [obtained from $S(q)$ in the 0.1–1 μm range], vs time, relative to quenchings to points $A-D$ of Fig. 1. Fractal dimensions are normalized to the final values d_g (Table I); times are normalized to the times of macroscopic gelation (Table II).

Two remarks are in order, related to these results: (i) No contradiction exists between our observed power law [Eq. (2)] and the monodispersity of demixed droplets expected during the Cahn-Hilliard linear regime [Eq. (1)]. This is because, as noted above, Eq. (2) shows to be valid in a scale interval well below $L_m/\sqrt{2}$, where Eq. (1) does not apply. The scale interval where we observe self-similarity, therefore, goes from above the size of an individual molecule, to well below the size of a demixed droplet. Consequently, the fractal dimension whose growth we observe is that which characterizes the structure of crosslinked polymers that self-assembles *within* the demixed, higher concentration, droplets.

(ii) Even within the interval specified above, using Eq. (2) would be incorrect in the presence of a fractal mass distribution of clusters. In our case, this is expected if spinodal demixing proceeds up to the coarsening stage. This, however, is confidently ruled out by noting from Table II that the time t_c corresponding to the end of the linear regime and the gelation time t_g (at which the demixed structure is frozen) are of the same order.

A summary, and comparison of the quantities characterizing the final structure of the gels and the relevant times characterising the different processes, is given in Tables I and II and in Fig. 10.

IV. DISCUSSION AND CONCLUSIONS

Kinetics of the three processes leading to gelation show distinct temperature dependences of absolute and relative values of their individual rates, for quenchings to points $A-D$ of the phase diagram of Fig. 1. In the following we shall refer to such quenchings simply as ''$A-D$.''

In *A* and *B*, spinodal demixing occurs first and establishes a mesoscopic pattern characterized by a correlation length of the order of several micrometers (Figs. 2 and 10). In the resulting higher concentration regions, conformational change and crosslinking are promoted [6,8,18–20]. This freezes-in the correlation length of the mesoscopic structure (Fig. 2) and causes the growth of the fractal structure of crosslinked polymers (Figs. 8 and 9). When crosslink percolation is reached, the fractal dimension of the crosslinked structure is also frozen in. However, further polymer diffusion and association still occurs, and gelation progresses within the constraints of a geometric frame frozen on the two ranges of length. Note that the peak of the structure function, $S(q_m)$ is proportional to $\langle \Delta c^2 \rangle$, and it is a measure of the degree of order or, better, of nonrandomness, in the system [19]. Its value proceeds growing well beyond the gel point, and more markedly and sharply in *A* than in *B*. As to conformational changes, Fig. 4 shows that the helical content at and beyond the gel point, very low in both cases, is much lower in *A* than in *B*. This correlates with the fact that the gel obtained in *B* is more rigid than that in *A*, by more than one order of magnitude (Fig. 7). Nevertheless, interesting information on the relation between conformational changes and crosslinking comes from a comparison of data of Figs. 4 and 6, relative to case *A*. The comparison shows that the G''/G' ratio has already decreased by about a factor 10 when conformational changes just become detectable. This shows that the helical content can depend upon the specific conditions

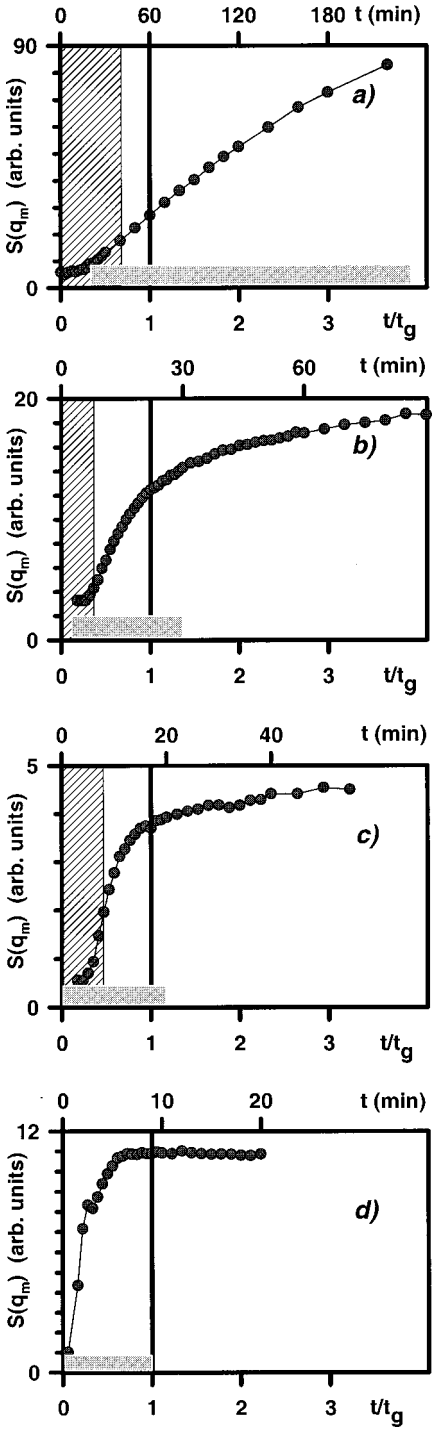

FIG. 10. Summary of kinetics relative to points *A* (a), *B* (b), *C* (c), and *D* (d) of Fig. 1, vs time, in gelation time units (lower scale). Real time in minutes is also given (upper scale). Circles, structure function at the maximum $S(q_m)$; hatched area, duration of Cahn's linear regime; vertical bar, onset of macroscopic gelation; gray horizontal bar, duration of the ORD growth, as per tracings of Fig. 4.

of gelation, and suggests the occurrence of some kind of crosslinks not necessarily requiring the formation of double or even simple helices. Crosslinking between highly extended helical chains [25(b)] possibly already existing in the sol [29] is indeed conceivable. This would agree with data on viscous dissipation suggesting the occurrence of weak long-range links in the demixed sol progressing towards gelation [7].

In *C*, demixing and conformational changes start simultaneously and concur in crosslinking, as shown by data in Figs. 2, 4, and 10. Once again, freezing in (due to crosslinking) of q_m and of d_f at its final d_g is observed in sequence. A lower $S(q_m)$, a broader peak and a still higher helical content and higher macroscopic rigidity characterize the final gel.

For quenching in *D*, the fastest process is the coil-helix conformational change (Figs. 4 and 10). No trace of demixing is seen in the structure function, just as for quenchings to the direct gelation region, away from the two-phase region of the sol. This shows that the development of a structure function is kinetically inhibited by crosslinking from the very beginning. Both the intensity of scattered light (which monitors concentration differences in the sample) and the ORD signal reach now their final value at the time of gelation. The entire average structure of the gel is now random, and does not show any characteristic scale length. Despite these differences, the fractal dimension and its time evolution are not different from those of the other cases (Table I and Fig. 9).

The low value of the final fractal dimension covers an interest of its own, as it is rare in the literature of fractal biomolecular aggregates [39]. The corresponding loose packing of aggregates concurs with demixing in making gelation possible at such low concentration. Ongoing experiments suggest that the same fractal dimension is observed in gels at both lower and higher Agarose concentrations.

The present observations of three different kinetic processes leading to the topological transition of gelation and of their multiple interactions illustrate new aspects of the complexity of gels and gelation. The frustrated nature of gels and, correspondingly, the complex role of kinetic competition among processes in determining the actual gelation path and final structure of gels are reflected in the ample diversity of structure and helical contents (and, perhaps, type) obtainable at a given polymer concentration by changing the quenching temperature only. However, unifying elements of simplicity emerge in terms of correlation length q_m^{-1}, degree of order, expressed by $S(q_m)$, and fractal dimension d_f. The latter reveals the role of geometry (fractal dimensionality), which turns out to be as significant as that of topology, all the more so if its freezing in at gelation is considered. In fact, the freezing in of d_f at its d_g value at gelation offers a new operational definition of ''gel point,'' in geometric rather than rheological terms.

A comment on the reported interplay of three processes is in order. Pairwise interactions between solution demixing, individual molecular conformational changes and crosslinking have been previously reported for the present system and for others [4–8,18–20]. The present experiments now offer a full view of multiple interactions and kinetic competitions among the three processes. The grounds for such multiple interactions are simply understood: (i) Solution demixing and polymer conformational changes can influence each other, because solvent-solute interactions play a strong role in both [21,40]. Accordingly, conformational changes altering the biomolecular surface exposed to the solvent can cause instability and demixing of the solution [4,5]. Reciprocally, biomolecular conformational changes can be favored

in high-concentration regions resulting from demixing, in consequence of non additivities [41] and related interaction changes. (ii) A similar two-way interaction exists between demixing and polymer crosslinking. The latter is in fact favored in higher concentration regions provided by demixing, while the demixed pattern is frozen in by the progress of crosslinking [4–8,18–20]. (iii) Analogously, molecular crosslinking and conformational changes can influence each other, because the latter can either provide or hide crosslinking sites or so-called hydrophobic contacts [5,8,9(b)], while crosslinking itself can of course interfere with further conformational changes. The three processes are therefore linked in principle by multiple path interactions. The present results show that prevailing of one or the other process or interaction depends upon kinetic competition under the given conditions. Consequently, competition is at least as significant as related energy scales *per se*, and it is responsible for the ample variety of gel structures that may correspond to one and the same point in the ''Gel'' region of the phase diagram of Fig. 1.

Finally, as we are observing the evolution of a system where spinodal demixing and gelation occur simultaneously and interfere, we should not expect and in fact we do not observe features predicted by spinodal demixing theory alone, nor features predicted by gelation theory alone. In particular, we note that gelation that starts inside the demixed droplets and freezes their distribution (quenchings to points *A*, *B*, and *C*) differs remarkably from direct (non-spinodal-assisted) gelation, because it occurs at *increasing* rather than at constant local concentration. This highlights an additional aspect of the concerted/competitive interaction of processes, and it stresses the interest of including kinetics in gelation theories.

The present results are also relevant to the fast growing field of pathological protein coagulation [9]. This is appreciated by considering that (i) a preliminary change leading to an ''intermediate'' molecular conformation is required for amyloid coagulation [9]; (ii) in Prion pathologies, infectious Prions can cause misfolding and participation in coagulation of host (non-intrinsically-pathogenic) prions. Interaction of the three microscopic and mesoscopic processes of demixing, conformational changes, and gelation (or extensive coagulation) has also been observed, although not kinetically, with bovine serum albumin [5], sickle cell hemoglobin HbS [4] and lysozyme (to be published), as well as with synthetic polypeptides [4]. Extensions of such studies, and of their kinetic aspects, currently in progress, suggest that these processes and their interactions could be rather common features of protein coagulation.

ACKNOWLEDGMENTS

We acknowledge partial support from local MURST and CRRNSM funds. We also thank D. Giacomazza for constant assistance and G. Lapis, M. Lapis, and R. Megna for technical help.

[1] P. G. de Gennes, *Scaling Concept in Polymer Physics* (Cornell University, Ithaca, NY, 1979).

[2] D. Stauffer, A. Coniglio, and M. Adam, Adv. Polym. Sci. **44**, 103 (1982).

[3] *Physical Networks*, edited by W. Burchard and S. B. Ross-Murphy (Elsevier, London, 1987); A. H. Clark and S. B. Ross-Murphy, Adv. Polym. Sci. **83**, 57 (1988); A. H. Clark, in *Biopolymer Mixtures*, edited by S. E. Harding, S. Hills, and J. R. Mitchell (Nottingham University Press, Nottingham, U.K., 1996), p. 37.

[4] (a) P. L. San Biagio and M. U. Palma, Biophys. J. **60**, 508 (1991); D. Bulone, P. L. San Biagio, M. B. Palma-Vittorelli, and M. U. Palma, Science **259**, 1335 (1993); (b) F. Sciortino, K. U. Prasad, D. W. Urry, and M. U. Palma, Biopolymers **33**, 743 (1993).

[5] P. L. San Biagio, D. Bulone, A. Emanuele, and M. U. Palma, Biophys. J. **70**, 494 (1996).

[6] (a) P. L. San Biagio, J. Newman, F. Madonia, and M. U. Palma, Chem. Phys. Lett. **154**, 477 (1989); (b) P. L. San Biagio, D. Bulone, A. Emanuele, F. Madonia, L. Di Stefano, G. Giacomazza, M. Trapanese, M. B. Palma-Vittorelli, and M. U. Palma, Makromol. Chem. , Macromol. Symp. **40**, 33 (1990); (c) A. Emanuele, L. Di Stefano, G. Giacomazza, M. Trapanese, M. B. Palma-Vittorelli, and M. U. Palma, Biopolymers **31**, 859 (1991).

[7] A. Emanuele and M. B. Palma-Vittorelli, Phys. Rev. Lett. **69**, 81 (1992); Int. J. Thermophys. **16**, 363 (1995); in *Flow-Induced Structure in Polymers*, edited by A. I. Nakatani and M. D. Dadmun (American Chemical Society, Washington, DC, 1995), p. 61.

[8] P. L. San Biagio, D. Bulone, A. Emanuele, M. B. Palma-Vittorelli, and M. U. Palma, Food Hydrocolloids **10**, 91 (1996).

[9] (a) J. Nguyen, M. A. Baldwin, F. E. Cohen, and S. B. Prusiner, Biochemistry **34**, 4186 (1995); (b) J. W. Kelly, Curr. Opin. Struct. Biol. **6**, 11 (1996); (c) M. F. Perutz, Nature (London) **385**, 773 (1997); (d) J. Safar, in *Prions, Prions, Prions*, edited by S. B. Prusiner (Springer, Berlin, 1998), p. 69; (e) J. I. Guijarro, M. Sunde, J. A. Jones, I. D. Campbell, and C. M. Dobson, Proc. Natl. Acad. Sci. USA **95**, 4224 (1998).

[10] J. Flory, J. Am. Chem. Soc. **63**, 3083 (1941); W. H. Stockmayer, J. Chem. Phys. **11**, 45 (1943); M. Gordon, Proc. R. Soc. London, Ser. A **268**, 240 (1962); A. Amemiya and O. Saito, J. Phys. Soc. Jpn. **26**, 1264 (1969).

[11] M. E. Fisher and J. W. Essam, J. Math. Phys. **2**, 609 (1961); J. W. Essam and K. M. Gwilym, J. Phys. C **4**, L228 (1971).

[12] S. Newman, W. R. Krigbaum, and D. K. Carpenter, J. Phys. Chem. **60**, 648 (1956); D. R. Paul, J. Appl. Polym. Sci. **11**, 439 (1967).

[13] A. Labudzinska and A. Ziabicki, Kolloid Z. Z. Polym. **243**, 21 (1971).

[14] T. Feke and W. Prins, Macromolecules **7**, 527 (1974).

[15] S. Wellinghoff, J. Shaw, and E. Baer, Macromolecules **12**, 932 (1979); M. Komatsu, T. Inoue, and K. Miyasaka, J. Polym. Sci., Polym. Chem. Ed. **24**, 303 (1986); P. Nunes and B. A. Wolf, Macromolecules **20**, 1952 (1987); X. He, J. Herz, and J. M. Guenet, *ibid.* **20**, 2003 (1987); **22**, 1390 (1989); T. Tanaka, G. Swislow, and I. Ohmine, Phys. Rev. Lett. **42**, 1556 (1979);

H. M. Tan, A. Moet, A. Hiltner, and E. Baer, Macromolecules **16**, 28 (1983); A. Coniglio, H. E. Stanley, and W. Klein, Phys. Rev. Lett. **42**, 518 (1979); Phys. Rev. B **25**, 6805 (1982); F. Tanaka and A. Matsuyama, *ibid.* **62**, 2759 (1989); F. Tanaka and W. H. Stockmayer, Macromolecules **27**, 3943 (1994).

[16] W. G. Miller, L. Kou, K. Tohyama, and V. Voltaggio, J. Polym. Sci., Polym. Symp. **65**, 91 (1978); K. Tohyama and W. G. Miller, Nature (London) **289**, 813 (1981); W. G. Miller, S. Chakrabarti, and K. M. Seibel, in *Microdomains in Polymer Solutions*, edited by P. Dubin (Plenum Press, New York, 1985), p. 143; P. S. Russo, P. Magestro, and W. G. Miller, in *Reversible Polymeric Gels and Related System*, edited by P. S. Russo (American Chemical Society, Washington, DC, 1987), p. 152; A. H. Chowdbury and P. S. Russo, J. Chem. Phys. **92**, 5744 (1990).

[17] S. Hayward, D. W. Heermann, and K. Binder, J. Stat. Phys. **49**, 1053 (1987).

[18] P. L. San Biagio, J. Newman, F. Madonia, and M. U. Palma, in *Biomolecular Stereodynamics III*, Proceedings of the Fourth Conversation in the Discipline Biomolecular Stereodynamics, State University of New York, Albany, NY, 1985, edited by R. H. Sarma and M. H. Sarma (Adenine Press, New York, 1986), p. 227; P. L. San Biagio, F. Madonia, J. Newman, and M. U. Palma, Biopolymers **25**, 2255 (1986).

[19] M. Leone, S. L. Fornili, and M. B. Vittorelli, in *Water and Ions in Biological Systems*, edited by L. Pullman, V. Vasilescu, and L. Parker (Plenum, New York, 1985), p. 677; M. Leone, F. Sciortino, M. Migliore, S. L. Fornili, and M. B. Palma-Vittorelli, Biopolymers **26**, 743 (1987).

[20] D. Bulone and P. L. San Biagio, Chem. Phys. Lett. **179**, 339 (1991); Biophys. J. **68**, 1569 (1995).

[21] P. J. Flory, *Principles in Polymer Chemistry* (Cornell University Press. Ithaca, NY, 1953).

[22] W. A. Eaton and J. Hofrichter, Adv. Protein Chem. **40**, 63 (1992).

[23] A. D. J. Rees, Adv. Carbohydr. Chem. Biochem. **24**, 267 (1969); S. Arnott, A. Fulmner, W. E. Scott, I. C. M. Dea, R. Moorhouse, and D. A. J. Rees, J. Mol. Biol. **90**, 269 (1974).

[24] I. T. Norton, D. M. Doodall, K. R. J. Austen, E. R. Morris, and D. A. J. Rees, Biopolymers **25**, 1009 (1985).

[25] a) S. A. Foord and E. D. T. Atkins, Biopolymers **28**, 1345 (1989); b) S. E. Schafer and E. S. Stevens, *ibid.* **36**, 103 (1995).

[26] G. Vento, M. U. Palma, and P. Indovina, J. Chem. Phys. **70**, 2848 (1979); P. L. Indovina, E. Tettamanti, M. S. Giammarinaro-Micciancio, and M. U. Palma, *ibid.* **70**, 2841 (1979).

[27] M. Manno and M. U. Palma, Phys. Rev. Lett. **79**, 4286 (1997).

[28] Y. Dormoy and S. Candau, Biopolymers **31**, 109 (1991).

[29] C. Rochas, A. Brulet, and J. M. Guenet, Macromolecules **27**, 3830 (1994).

[30] P. N. Pusey and W. van Megen, Physica A **157**, 705 (1989).

[31] K. Kubota and N. Kuwahara, Jpn. J. Appl. Phys., Part 1 **31**, 3740 (1992).

[32] J. W. Cahn, J. Chem. Phys. **42**, 93 (1965).

[33] S. Langer, M. Bar-on, and H. D. Miller, Phys. Rev. A **11**, 1417 (1975); E. Siggia, *ibid.* **20**, 595 (1979); H. Furukawa, Adv. Phys. **34**, 703 (1985).

[34] R. Bansil, J. Lal, and B. Carvalho, Polymer **33**, 2961 (1992); F. Sciortino, R. Bansil, H. E. Stanley, and P. Alstrøm, Phys. Rev. E **47**, 4615 (1993).

[35] M. Doi and S. F. Edwards, *The Theory of Polymer Dynamics* (Oxford University Press, Oxford, 1986).

[36] P. G. de Gennes, J. Chem. Phys. **55**, 572 (1971).

[37] B. Zimm, J. Chem. Phys. **24**, 269 (1956).

[38] S. K. Sinha, Physica D **38**, 310 (1989); P.-z. Wong and Q.-z Cao, Phys. Rev. B **45**, 7627 (1992).

[39] M. Dahmani, M. Skouri, J. M. Guenet, and J. P. Munch, Europhys. Lett. **26**, 19 (1994); P. Wiltius, *Kinetics of Aggregation and Gelation*, edited by F. Family and D. P. Landau (Elsevier, Amsterdam, 1984), p. 261; D. L. Tipton and P. S. Russo, Macromolecules **29**, 7402 (1996).

[40] C. B. Post and B. H. Zimm, Biopolymers **21**, 2123 (1982).

[41] F. Brugé, S. L. Fornili, G. G. Malenkov, M. B. Palma-Vittorelli, and M. U. Palma, Chem. Phys. Lett. **254**, 283 (1996); V. Martorana, G. Corongiu, and M. U. Palma, *ibid.* **254**, 292 (1996); D. Bulone, V. Martorana, P. L. San Biagio, and M. B. Palma-Vittorelli, Phys. Rev. E **56**, R4939 (1997); P. L. San Biagio, D. Bulone, V. Martorana, M. B. Palma-Vittorelli, and M. U. Palma, Eur. Biophys. J. **27**, 183 (1998).